

Synchrotron micro-X-ray fluorescence analysis of natural diamonds: First steps in identification of mineral inclusions in situ

HUSIN SITEPU,^{1,*} MAYA G. KOPYLOVA,^{1,†} DAVID H. QUIRT,² JEFFREY N. CUTLER,³
AND THOMAS G. KOTZER³

¹Department of Earth and Ocean Science, The University of British Columbia, Vancouver, British Columbia V6T 1Z4, Canada

²Saskatchewan Research Council, 15 Innovation Boulevard, Saskatoon, Saskatchewan S7N 2X8, Canada

³Canadian Light Source Inc., 101 Perimeter Road, Saskatoon, Saskatchewan S7N 0X4, Canada

ABSTRACT

Diamond inclusions are of particular research interest in mantle petrology and diamond exploration as they provide direct information about the chemical composition of upper and lower mantle and about the petrogenetic sources of diamonds in a given deposit. The objective of the present work is to develop semi-quantitative analytical tools for non-destructive in situ identification and characterization of mineral inclusions in diamonds using synchrotron micro-X-ray Fluorescence (μ SXRF) spectroscopy and micro-X-ray Absorption Near Edge Structure (μ XANES) spectroscopy at a focused spot size of 4 to 5 micrometers. The data were collected at the Pacific Northwest Consortium (PNC-CAT) 20-ID microprobe beamline at the Advanced Photon Source, located at the Argonne National Laboratory, and yielded the first high-resolution maps of Ti, Cr, Fe, Ni, Cu, and Zn for natural diamond grains, along with quantitative μ SXRF analysis of select chemical elements in exposed kimberlite indicator mineral grains. The distribution of diamond inclusions inside the natural diamond host, both visible and invisible using optical transmitted-light microscopy, can be mapped using synchrotron μ XRF analysis. Overall, the relative abundances of chemical elements determined by μ SXRF elemental analyses are broadly similar to their expected ratios in the mineral and therefore can be used to identify inclusions in diamonds in situ. Synchrotron μ XRF quantitative analysis provides accurate estimates of Cr contents of exposed polished minerals when calibrated using the concentration of Fe as a standard. Corresponding Cr K-edge μ XANES analyses on selected inclusions yield unique information regarding the formal oxidation state and local coordination of Cr.

INTRODUCTION

The exceptional chemical and physical properties of diamond allow it to store and preserve information about the deep mantle from which it originates. Diamond crystals often incorporate grains of other minerals as they grow, and shield these mineral inclusions from later destruction. These diamond inclusions (DIs) record information about the mineralogy, composition, and thermal regime of the ancient Archean-Proterozoic lithospheric mantle, thus providing constraints on processes that lead to stabilization of proto-continent. In addition, diamonds and DIs provide valuable information for diamond exploration programs, allowing determination of diamond parent paragenesis (eclogitic or peridotitic; Gurney 1989) and leading to prioritization of exploration targets.

Historically, DIs have been studied by destructive methods in which the diamonds are crushed (Sobolev et al. 1970; Gurney et al. 1984; Gurney 1989) or ablated (Seitz et al. 2003), thereby destroying all smaller inclusions and extracting only parts of larger

inclusions. The recovered inclusions are then mounted on a slide, polished, and analyzed using electron microprobe techniques. This complicated and time-consuming process requires 2–3 days to study major mineral inclusions in just one diamond.

Synchrotron micro-X-ray Fluorescence (μ SXRF) spectroscopy is an established method for non-destructive extraction of important chemical and mineralogical information from fluid and solid inclusions in minerals (Frantz et al. 1988; Mavrogenes et al. 1995). The utility of the synchrotron micro-techniques is enhanced by the high brightness and energy of the third-generation synchrotron sources (Sutton et al. 2002), such as the Advanced Photon Source (APS) and the Canadian Light Source (CLS), and by the high spatial resolution of the associated microprobe beamline and end-station. It takes only minutes to collect a fluorescence spectrum from a high intensity X-ray beam produced by synchrotron radiation and, due to its substantial penetration depth, synchrotron μ XRF can probe inclusions in situ. Moreover, with recent advances in micro-focusing techniques, one can collect a meaningful μ SXRF signal from 5–10 μ m inclusions (Vincze et al. 2004) that previously could not be characterized.

Mineral inclusions in diamonds have been studied with the μ SXRF technique qualitatively (Ohigashi et al. 2002; Meng et al. 2003) and, most recently, quantitatively (Vekemans et al. 2004; Vincze et al. 2004). Quantification of the μ SXRF data

* Present address: Crystallography Laboratory, Department of Geosciences, Virginia Tech, Blacksburg, VA 24061. E-mail: sitepu@vt.edu

† E-mail: mkopylov@eos.ubc.ca

requires knowledge of the geometry of an individual inclusion and its position in the host mineral. These two parameters could be determined optically (Mavrogenes et al. 1995; Rickers et al. 2004) or extracted from the fluorescence spectrum (Philippot et al. 1998) and transmission line scans (Cauzid et al. 2004). Concentrations of trace elements are then evaluated by reference to an external or internal standard (Mavrogenes et al. 1995; Vincze et al. 2004; Hansteen et al. 2000) or by comparison with spectra simulated by a Monte Carlo routine (Rickers et al. 2004). Such quantitative analysis, however, has a limited application to mantle petrology and diamond exploration as it provides only trace element abundances (i.e., elements with $Z > 20$), but does not allow mineral identification.

The aim of this study is to optimize the μ SXRF technique for diamond exploration that requires non-destructive qualitative determination of mineral inclusions hosted by diamonds. We tested if μ SXRF method could identify DI in situ based on simple semi-quantitative treatment of XRF spectra. Furthermore, we used several elements in natural diamond indicator minerals for internal standardization and assessed the uncertainties, sensitivity, and limitations of such quantitative μ SXRF analysis. We also evaluated the utility of the Absorption Near Edge Structure (μ XANES) spectroscopy for identification and characterization of mineral inclusions in diamonds. Our study reports the first μ SXRF chemical distribution maps of natural diamonds and DIs and extends our knowledge of metal impurities in diamonds from artificial (Meng et al. 2003) to natural samples.

MATERIALS AND ANALYTICAL METHODS

Synchrotron X-ray fluorescence data were acquired for two kinds of natural grains: (1) diamonds from the Jericho kimberlite (NWT, Canada) and (2) kimberlite indicator minerals. All the grains were polished with 600–3 μ m pastes to a standard quality required for the electron microprobe analysis. Three diamonds (372X, 280RS, and 344X), up to approximately 3 mm in size and containing inclusions of purple harzburgitic garnet, orange eclogitic garnet, green clinopyroxene, opaque sulfide, and numerous colorless inclusions, were investigated. The inclusions, where possible, were exposed by polishing away the host diamond and then analyzed on a fully automated CAMECA SX-50 electron microprobe (Earth and Ocean Sciences Department, UBC), operating in the wavelength-dispersion mode with the following operating conditions: excitation voltage, 15 kV; beam current, 20 nA; peak count time, 10s; beam diameter, 3 μ m. The electron microprobe data were reduced using the "PAP" $\phi(\rho Z)$ correction procedure. Several selected kimberlite indicator minerals were also analyzed by μ SXRF for use as reference minerals in subsequent elemental quantification evaluations. The kimberlite indicator minerals are chromite (Chromite 9-12, Table 1A) from Jericho peridotite xenoliths and eclogite garnet (Eclogitic Garnet YK 2416, Table 1A) and green clinopyroxene (Cr-diopside YK 2416, Table 1). Electron microprobe analyses (EMP) of the chromites are reported in McCammon and Kopylova (2004). The garnet and clinopyroxene were analyzed using a JEOL 8600 Superprobe (Department of Geological Sciences, University of Saskatchewan). The probe was operated at an accelerating voltage of 15 kV, beam current of 50 nA, take off angle of 40°, and a beam diameter of ~5 μ m. Grains of natural Cr-diopside, olivine, and pyrope were used as standards. All elements were counted for 100 s. Matrix and ZAF corrections were performed using formulas modeled after Heinrich/Duncumb-Reed.

Synchrotron μ SXRF elemental distribution maps and Cr K-edge μ XANES spectra were collected at the APS Pacific Northwest Consortium Collaborative Access Team (PNC-CAT) 20-ID beam line using an energy of 11.8 keV ($\lambda = 1.05085$ nm). The PNC-CAT spectrometer has been described in detail by Heald et al. (2001). X-rays exiting the Si(111) double-crystal monochromator were at an incident angle of 45° to the sample. The samples were placed on Kapton tape and mounted on a high-precision x-y translation stage. The resolving power of the monochromator was approximately 10000 and a Kirkpatrick-Baez mirror pair (Eng et al. 1995) focused the beam to a spot size of approximately 4 μ m \times 5 μ m. This spot size limits the spatial resolution of the method. As the analytical setup was open to

the atmosphere, significant attenuation of the lower-energy X-rays in the air path to the detector occurred and only the fluorescence data for elements heavier than Ca (such as Ti, Cr, Fe, Ni, Cu, and Zn) was collected. The μ SXRF spectra were collected using a 7-element intrinsic Ge detector mounted at 90° to the incident beam (45° to the sample normal). This 45° incident angle to the sample is within the 40–60° range recommended for the optimal set-up of analytical μ SXRF (Cauzid et al. 2004). Spectral reproducibility was excellent among repeat μ SXRF spectra. Elemental distribution maps of Ti, Cr, Fe, Ni, Cu, and Zn were obtained using a step size of 10–15 μ m and counting times of 0.5 s/step, resulting in maximum data acquisition times of approximately 9 hours. Estimated detection limits for these analytical conditions range from approximately 100 ppm for Ti ($Z = 22$) to around 10 ppm for Zn ($Z = 27$). μ SXRF spot analysis spectra of DIs and kimberlite indicator mineral grains were integrated over a 60 s collection period, yielding lower detection limits of around 10 ppm for Ti to less than 1 ppm for Zn.

μ SXRF spectroscopy is a volume analysis technique. It records an integrated signal from excited atoms distributed within the 3D analytical volume of material. The technique, therefore, depends little on the quality of the material surface. The main restriction on the analytical penetration depth is X-ray absorption of the incident and fluorescent beams by the host material and the inclusion itself (Frantz et al. 1988). The XRF signals that we analyzed were derived mainly from the upper half of the samples as incident X-rays attenuate exponentially when passing through matter. Diamond, however, shows less attenuation and absorption of X-rays than other common minerals as it is made of lighter carbon atoms. It was estimated that an 8.6 keV X-ray beam decreases in intensity by more than 40% after passing through a 0.35 mm diamond layer (Meng et al. 2003). In a given matrix, the maximum analytical depth of the technique depends on the X-ray excitation energy and on the concentration and characteristic X-ray fluorescence of an element. Elements with X-ray energies closer to the excitation energy can be detected in lower concentrations, and lighter elements can only be analyzed in shallower inclusions (Mavrogenes et al. 1995). For example, Sr X-ray fluorescence from in situ diamond inclusions is completely attenuated in a 200 μ m diamond layer, whereas Zr becomes undetectable below a 275 μ m diamond layer using a 28 keV X-ray beam energy (Vekemans et al. 2004). With a 8.3 keV X-ray excitation energy, Fe inclusions were detected in a 0.5 mm diameter diamond (Ohgashi et al. 2002). In our study, the excitation energy of 11.8 keV allowed detection of measurable Fe, Mn, Ni, Cu, Zn, Co, Cr, and Ti in inclusions located in the upper 0.5 mm diamond layer as determined optically.

μ XANES analysis, using focused spot sizes of 4 to 5 μ m, was done on several of the inclusions following acquisition of the elemental distribution maps. Fluorescence μ XANES spectra were collected at the Cr K-edge (1s) absorption edge ($E_0 = 5989$ eV) on selected areas on the diamond inclusions, reference minerals and Cr foil. Cr K-edge μ XANES spectra were collected over the pre-edge region (5850 to 5979 eV) using a step size and dwell time of 8 eV and 2 s, respectively and across the absorption edge (5980–6280 eV) using a step size and dwell time of 0.25 eV and 2 s, respectively. All μ XANES spectra collected were calibrated using pure Cr foil ($E_0 = 5989$ eV).

Data reduction

To quantify the data, synchrotron μ SXRF spectra were deconvoluted using a Levenburg-Marquardt non-linear minimization algorithm (Bevington 1969), taking into account a quasi-linear baseline. The areas of the fitted peaks were determined using PeakFit 4.12 program developed by SeaSolve Software (<http://www.systat.com/products/PeakFit/>) and the ratios of the areas semi-quantitatively characterize the minerals (Table 1A).

Quantification of the elemental concentrations was done using SNRLXRF software (Sutton et al. 2002), a modification of NRLXRF developed by the Naval Research Laboratory (Birks et al. 1977; Criss et al. 1978), which converts elemental peak areas into absolute concentrations using theoretical predictions of fluorescence intensity assuming that the concentration of one constituent is known. A sensitivity analysis of the software corrections on the resulting element concentrations was carried out by varying several input parameters, such as the reference element concentration, mineral density, and grain thickness (Table 1B). The primary sources of error are the uncertainties in the peak areas derived from the peak fitting routine and in the reference element concentration, while minor changes in mineral density and grain thickness have little impact on the final result.

Using the electron microprobe Fe concentration as the reference element in the SNRLXRF quantification routine, the calculated Cr contents of the kimberlite indicator minerals agree well with the electron microprobe data (Table 1A). Accuracy of the Cr analysis is calculated to be 1.2–13.1 rel%, which is similar to the 0.2–14.0 rel% accuracy of the μ SXRF analysis of elements with $Z = 29$ –92,

TABLE 1A. Chemical compositions and element ratios for DIs and indicator minerals analysed by electron microprobe (EMP) and micro-SXRF

Mineral	Cr (wt%)		Fe (wt%)		Ti (wt%)		Ni (wt%)	
	EMP	μ XRF*	EMP	μ XRF*	EMP	μ XRF*	EMP	μ XRF*
Using Fe as reference element								
Chromite 9-12	37.32	37.77	17.25	17.25	0.05	n/d ¹	n/d	n/d
Eclogitic garnet YK-2416	3.81	2.32	5.65	5.65	0.11	n/d	0.00	n/d
Cr-diopside YK-2416	0.31	0.08	2.80	2.80	0.11	n/d	0.02	n/d

Mineral	Element Ratios [100*(element/Fe)]								EMP summary	XRF summary	
	Cr			Ti		Mn		Ni			
	EMP	μ XRF*	μ XRF [†]	EMP	μ XRF [†]	EMP	μ XRF [†]	EMP			μ XRF [†]
Chromite 9-12	216.4	219.0	296.65	0.29	n/d	0.34	n/d	0.31	n/d	Cr>Fe>Ti=Mn=Ni	Cr>Fe>Ti=Mn=Ni
Eclogitic garnet YK-2416	67.4	41.1	27.28	1.95	n/d	5.61	n/d	0.07	n/d	Fe>Cr>>Mn>Ti>Ni	Fe>Cr>>Mn=Ti=Ni
Cr-diopside YK-2416	11.0	2.86	6.12	3.79	n/d	3.27	n/d	0.79	n/d	Fe>Cr>Mn=Ti>Ni	Fe>Cr>Mn=Ti=Ni
diamond 372X inclusion 1 (eclogitic Cpx)	0.8	n/d	n/d	2.4	n/d	1.3	n/d	0.58	1.82	Fe>>Ti=Cr=Mn=Ni	Fe>>Ti=Cr=Mn=Ni
diamond 372X inclusion 2 (eclogitic Gar+sulfide)	0.2	n/a	n/d	1.0	n/d	1.8	1.19	>0.5	17.9	Fe>>Ti=Cr=Mn=Ni	Fe>Ni>Mn>Ti=Cr
diamond 280RS inclusion 1 and 2 (sulfides)	0.04-0.08	n/a	24.06	0.04-0.08	n/d	0.04-0.08	n/d	71-139	103.3	Fe=Ni>>Cr=Ti=Mn	Fe=Ni>>Cr>Ti=Mn
diamond 344X inclusion 1 (peridotitic Grt)	25-60	n/a	38.1	0.4-3	n/d	3.5-4.9	1.83	0.5-2.5	n/d	Fe>Cr>>Mn>Ti=Ni	Fe>Cr>>Mn>Ti=Ni
diamond 344X inclusion 2 (olivine)	0.30	n/a	1.43	0.20	n/d	0.7-1.1	0.97	4.4-5.2	n/d	Fe>>Ni>Cr=Mn=Ti	Fe>>Cr=Mn>Ti=Ni

* Element ratios obtained using SNRLXRF wt% data.

[†] Element ratios obtained using μ XRF peak area values.**TABLE 1B.** SNRLXRF sensitivity analysis using Fe as the reference element

SNRLXRF sensitivity analysis	Fe, wt%	item rel%	Cr rel% var.
delta Fe = 0.5 wt%	Chromite 9-12	17.25	2.90
	Eclogitic garnet YK-2416	5.65	8.85
	Cr-diopside YK-2416	2.8	17.86
delta density = 0.5 g/cm ³	n/a	10.0	0.00
delta thickness = 0.2 mm	n/a	20.0	0.00

Notes: Qualitative elemental ratios for diamond inclusions in the EMP column (except 372X DI1) are estimated based on general composition on typical garnets, olivine, clinopyroxene and sulfides associated with diamonds in the Jericho xenoliths reported in Kopylova et al. (1999a, b). Eclogitic clinopyroxene 372X DI2 is analysed at the EOS department at UBC. n/d = not detected; n/a = not applicable/analyzed.

with quantification achieved by reference to a standardized element (Hansteen et al. 2000). For Cr content in indicator minerals, we compared elemental ratios based on μ SXRF PeakFit peak areas with the ratios based on SNRLXRF software. While Cr estimates in chromite and garnet are greatly improved by the SNRLXRF quantification, the Cr content in Cr-diopside is more accurate for the μ XRF PeakFit data reduction (Table 1A). Good spectral reproducibility of this study indicated that precision of our μ SXRF data is comparable with that reported in other μ SXRF studies with external or internal standards, i.e., from 8% (Philippot et al. 1998) to 10-39 rel% (Mavrogenes et al. 1995).

RESULTS AND DISCUSSION

μ SXRF analysis

Figure 1-3 show high-resolution, false color elemental distribution maps of I_t (transmitted beam attenuation), and Ti, Cr, Fe, Ni, Cu, and Zn fluorescence for Jericho diamonds 372X, 280RS, and 344X along with XRF spectra of selected DIs. It is immediately evident that the elemental distribution is heterogeneous and inclusions with sizes of approximately 10 μ m, which are not visible using transmitted light microscopy, are clearly visible. The μ SXRF signal originated mainly from within the upper ~0.5 mm of diamond grains and thus delineates the precise location and chemical composition of exposed and non-exposed inclusions in situ. Contents of Ti, Cr, Fe, Ni, Cu, Zn, and Sr in the host diamonds, although low and variable, are often above the minimum detection limit of approximately 5-10 ppm, under these analytical conditions, of the μ XRF technique (Quirt 2003).

Diamond 372X hosts numerous inclusions of green eclogitic clinopyroxenes (i.e., DI1 on Fig 1E) and one grain of light orange

eclogitic garnet (DI2 on Fig 1E). The inclusions contain high and variable amounts of Fe (Figs. 1I and 1J) and minor Ni (Fig. 1I), Cr (Fig. 1C), and Ti (Fig. 1D). The garnet has higher Fe than the clinopyroxene inclusion (Table 1A), in accordance with the typical compositions of Jericho eclogitic minerals (Kopylova et al. 1999a). Ni content of the garnet grain is higher due to the accidental presence of sulfide flakes optically detectable around the inclusion. Diamond 372X itself demonstrates an interesting pattern of heterogeneous distributions of Ni and Cu. These elements show relatively elevated concentrations only in one part of the diamond, separated from the rest of the diamond by a straight boundary (Figs. 1G and 1H). We ascribe this pattern to differing levels of Ni and Cu in a twinned diamond crystal or in various diamond growth zones as the diamond was carefully checked and showed that it is a single grain, not a polycrystal. The presence of more than 8 ppm Ni (the approximate MDL for a counting time of 0.6 s) in a natural diamond is rare and more often is restricted to synthetic diamonds (Meng et al. 2003).

Diamond 280RS hosts several opaque sulfide grains. All mineral inclusions contain similarly high amounts of Fe and Ni (Fig. 2I), minor Ti (Fig. 2D), Cu and Zn (Fig. 2I). The largest two inclusions depicted in Figures 2B and 2C were plucked and/or polished out during polishing and the elemental maps in Figure 2 therefore show lower concentrations of Fe and Cr in the central parts of the inclusions. Smaller inclusions annotated as 1 and 2 have similar compositions based on μ SXRF spectra (Fig. 2I and Table 1A); high contents of siderophile elements

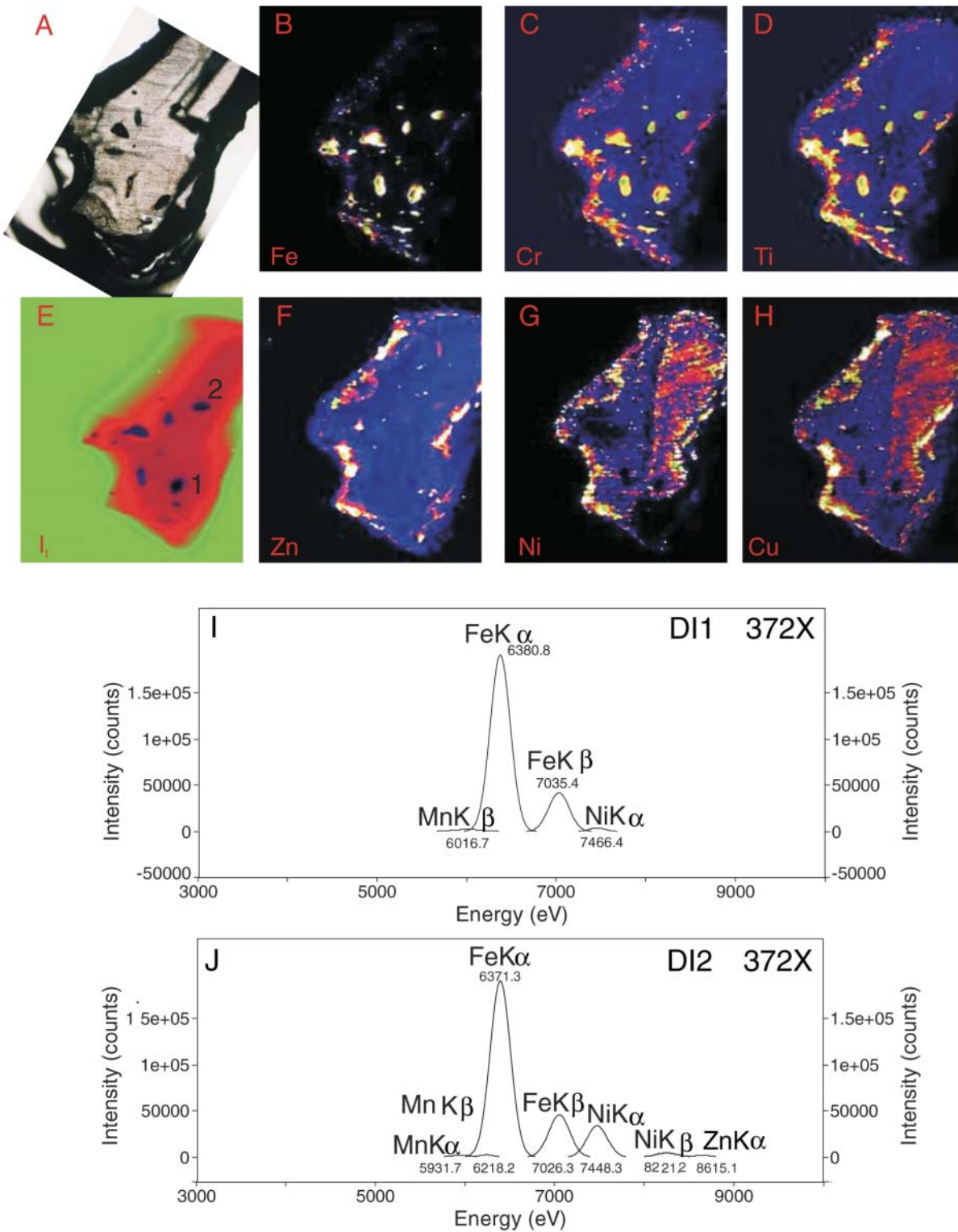


FIGURE 1. Optical image, μ XRF maps, and inclusion chemistry of diamond 372X. (A) Optical image; specimen is 3.05 mm in maximum dimension. Images (B-D) and (F-H) are false color maps for Fe, Cr, Ti, Zn, Ni, and Cu, with horizontal and vertical sides of 2650 μ m and 1700 μ m, respectively, with a step size of 15 μ m. On all X-ray maps of Figures 1–3, the brightness of the colors is proportional to element concentration. Location of spectra is shown on the corresponding I_r density map (E). (I) Results of PeakFit deconvolution of μ XRF spectra for inclusions DI1 and DI2.

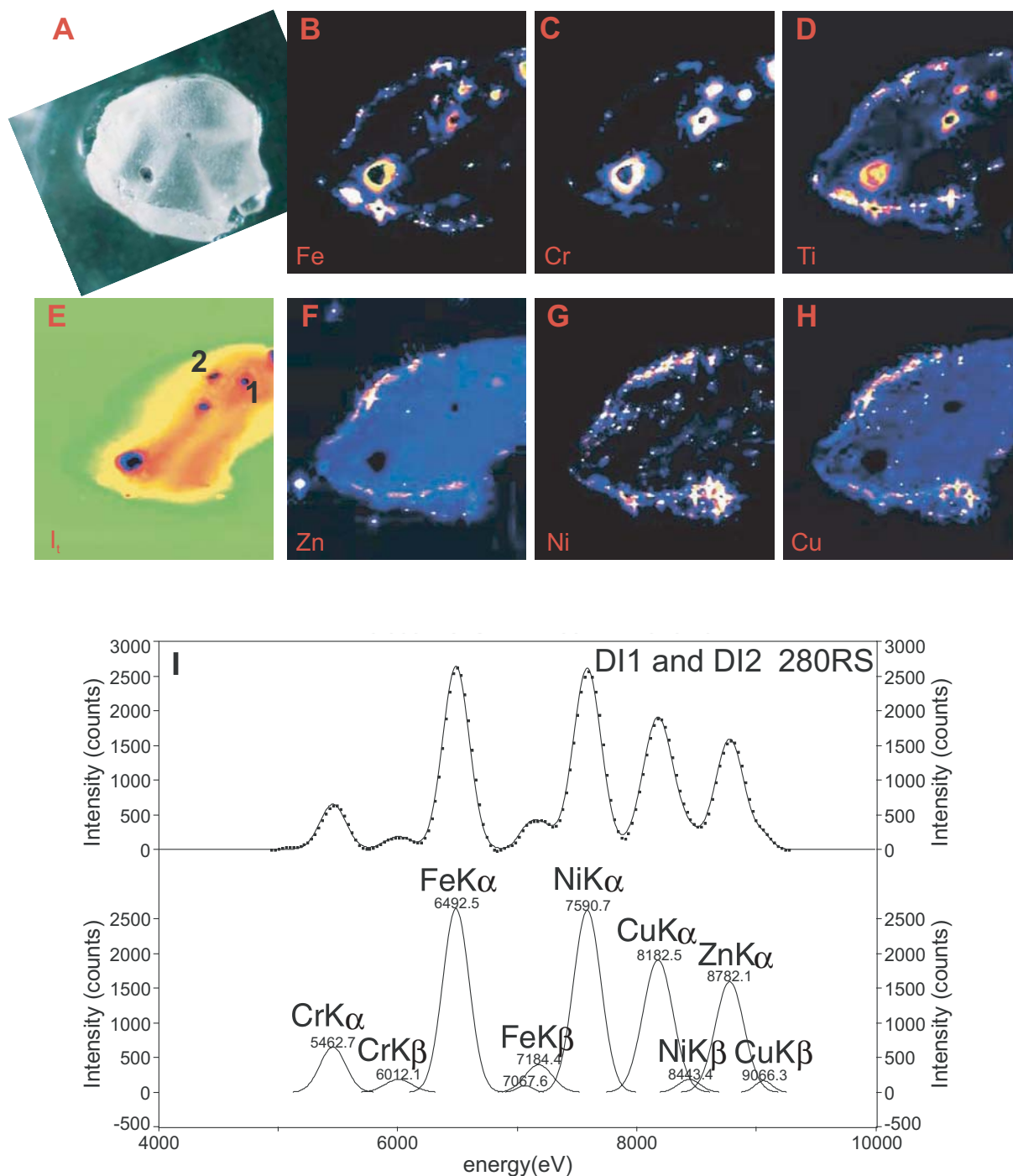


FIGURE 2. Optical image, μ XRF maps, and inclusion chemistry of diamond 280RS. (A) Optical image; specimen is 1.70 mm in diameter. Images (B–D) and (F–H) are false color maps for Fe, Cr, Ti, Zn, Ni, and Cu, with horizontal and vertical sides of 2000 μ m and 1200 μ m, respectively, and a step size of 10 μ m. Location of spectra is shown on the corresponding I_1 density map (E). (I) An original spectrum and results of PeakFit deconvolution of μ XRF spectrum for inclusions DI1 and DI2.

Ni, Cu, and Zn classify them as sulfides.

Diamond 344X hosts one large inclusion of purple peridotitic garnet and at least one smaller colorless inclusion, most likely olivine. Both stand out from the diamond matrix by displaying

elevated contents of Fe (Fig. 3 B, F, G), Cr (Fig. 3C), and Ti (Fig. 3E), and they contain detectable amounts of Mn and Co (Fig. 3F). The peridotitic garnet (inclusion 1 — Fig 3D) has high contents of Fe and Cr (Fig. 3F), while olivine (inclusion 2 — Fig 3D) is

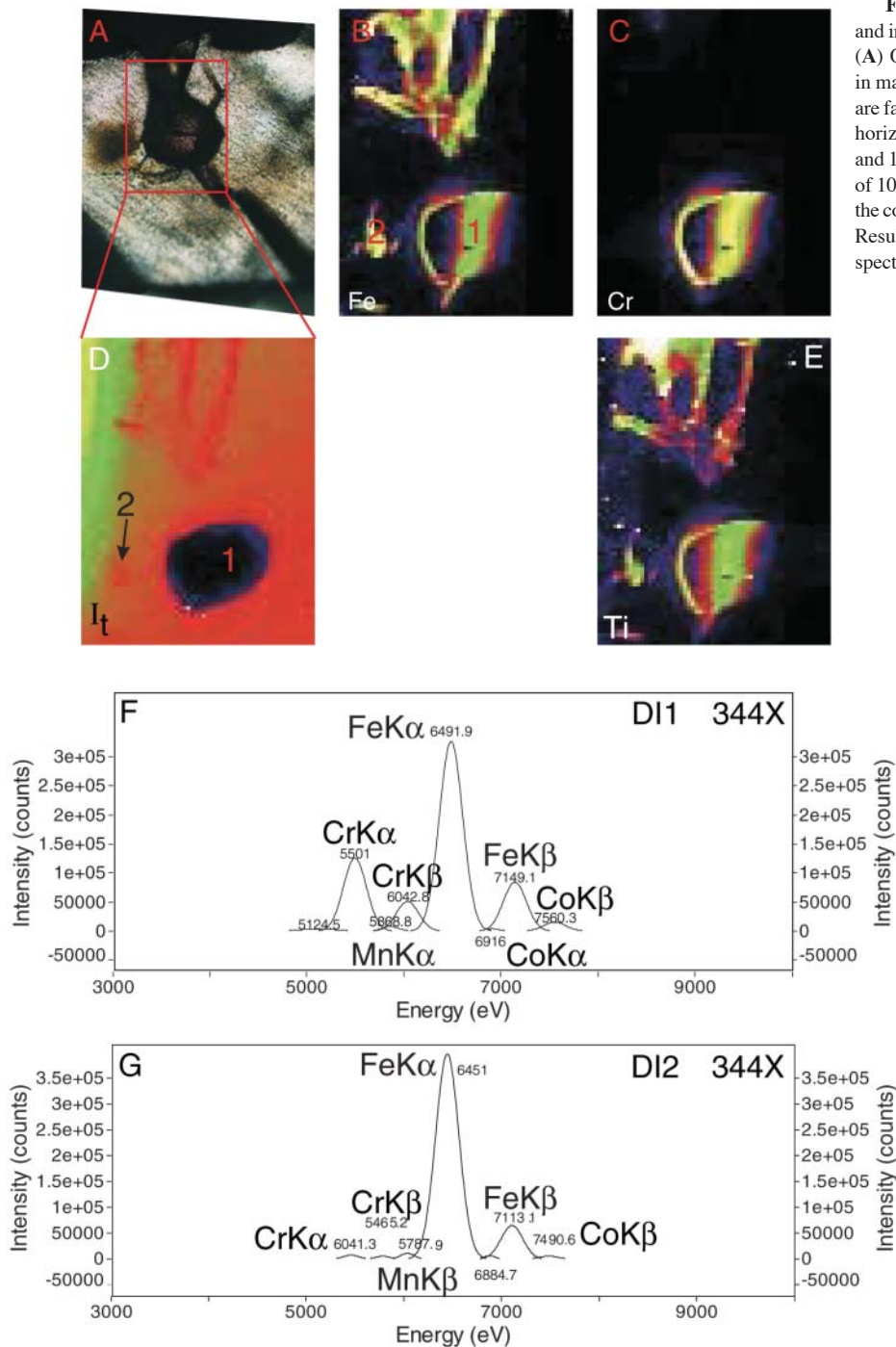


FIGURE 3. Optical image, μ XRF maps, and inclusion chemistry of diamond 344X. (A) Optical image; specimen is 2.00 mm in maximum dimension. Images (B, C, E) are false color maps for Fe, Cr, and Ti, with horizontal and vertical sides of 2100 μ m and 1500 μ m, respectively, with a step size of 10 μ m. Location of spectra is shown on the corresponding I_t density map (D). (F, G) Results of PeakFit deconvolution of μ XRF spectra for inclusions DI1 and DI2.

Fe-rich and is significantly lower in Cr content (Fig. 3G). The ratios of elemental peak areas for inclusions 1 (Cr/Fe = 38) and 2 (Cr/Fe = 1.4; Table 1) match well their optical classification and general compositions of DI (Table 1A). In Jericho xenolithic peridotites, and in cratonic peridotites in general, only olivine is richer in Fe than Cr-pyrope (Kopylova et al. 1999b).

In all analyzed diamonds, the ratios of the elemental peaks in μ XRF spectra can qualitatively identify even non-exposed

inclusions in diamonds, as the relative abundances of the elements in the μ XRF spectra are broadly similar to their expected ratios (Table 1A). In all 8 minerals where a comparison between electron microprobe and μ XRF analyses were possible, the relative abundances of elements summarized in the last two columns of Table 1A are close. The results agree well with minor selective self-absorption of the elemental XRF expected in the light diamond matrix for elements with a limited range of atomic

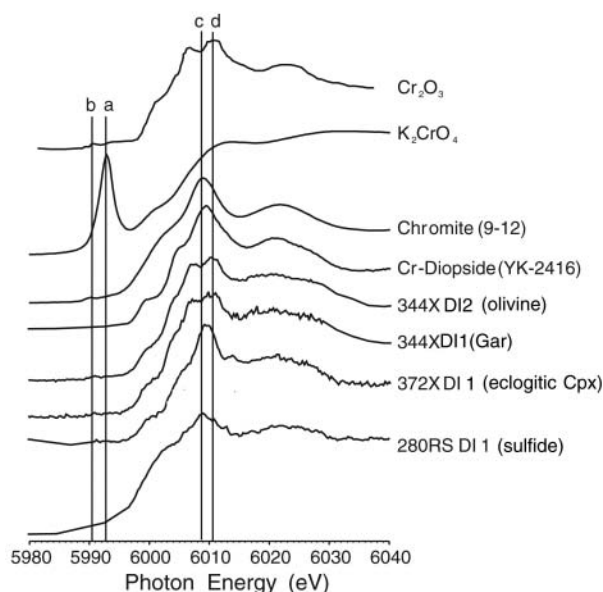


FIGURE 4. Cr K-edge XANES Spectra for reference standards (Cr_2O_3 , K_2CrO_4), reference chromite (Chromite 9-12) and chrome diopside minerals (Cr-Diopside, YK-2416) and micro-inclusions from diamond samples 280RS, 344X, and 372X. Locations of inclusions in diamonds are shown in Figures 1 to 3. Solid vertical lines designate photon energy positions for (a) pre-edge Cr^{6+} absorption peak, (b) Cr^{3+} pre-edge absorption peak, (c) main absorption edge for Cr^{3+} in spinel structure (~ 6008.5 eV; Levy et al. 1999) and (d) main absorption edge for Cr^{3+} in corundum structure (~ 6011 eV; Levy et al. 1999).

numbers $Z = 22-27$.

We conclude that (1) the distribution of diamond inclusions inside the natural diamond host, both visible and invisible using optical transmitted-light microscopy can be mapped with synchrotron μXRF analysis, and (2) synchrotron μXRF quantitative analysis provides accurate estimates of Cr contents of exposed polished minerals when calibrated using the concentration of Fe as a standard.

μXANES analysis

Cr K-edge μXANES analyses on selected diamond inclusions, reference compounds and supplied indicator minerals (Fig. 4) have been used to (1) provide unique information regarding the formal oxidation state of Cr in the inclusions and (2) characterize the localized chromium structural environment. None of the Cr K-edge μXANES spectra for the reference indicator minerals (Chromite 9-12; Cr-Diopside YK-2416; Fig. 4) and diamond inclusions (DI samples, Fig. 4) contain an absorption band at approximately 5993 eV (line a on Fig. 4), indicative of the presence of hexavalent Cr in a tetrahedral coordination, as in potassium dichromate (K_2CrO_4).

In general, two types of Cr K-edge μXANES spectra can be distinguished. Spectra with one main absorption feature at approximately 6008.5 eV (line c, Fig. 4), and spectra with split peaks around 6010 (line d, Fig. 4) and 6006 eV. Similar Cr absorption edge positions were documented by Levy et al. (1999) wherein Cr K-edge XANES analyses on Cr^{3+} in natural and synthetic mineral compounds indicated one or two Cr-O

bond distances, typical of spinel and corundum structures, respectively. Cr K-edge XANES spectra in this study have been interpreted to represent Cr^{3+} occurring in regular octahedrons (equal Cr-O bond distances, spinel structure) or distorted octahedrons (unequal Cr-O bond distances, corundum structure). This is reasonable based on the crystallography and compositions of the minerals analyzed. Synthetically prepared garnets at 1200 °C have chromium K-edge XANES spectra suggesting Cr^{3+} in distorted octahedrons (Gunsser et al. 1994). Olivine minerals have both distorted and regular octahedrons (Klein and Hurlbut 1993), both of which can contain Cr^{3+} (Taura et al. 1998) and could yield Cr K-edge XANES spectra similar to that of either spinel or corundum structure. Cr K-edge XANES on crystal lattices of chromite and diopside (Cabaret et al. 1998; Levy et al. 1999; Cloutis 2002) suggest Cr^{3+} coordination comparable with regular octahedral coordination of Cr in a spinel structure, which is in agreement with the Cr K-edge μXANES spectra for chromite (9-12), Cr-diopside (YK-2416) and eclogitic clinopyroxene (Fig. 4).

Extension of these spectral-crystallographic relations to the Cr K-edge μXANES spectra for DI in this study provide information regarding the structural coordination of Cr^{3+} and may be linked broadly with DI mineralogy and chemical analyses. For instance, elemental ratios from μSXRF (Table 1A), supportive of sample 344X DI1 and 344X DI2 being previously identified as peridotitic garnet and olivine, respectively, yields Cr K-edge μXANES spectra expectable, although non-unique, for these minerals. We conclude that μXANES spectra provide accurate information about the valence state and local structure of Cr for DI in situ, but has limited utility for identification of DI minerals.

ACKNOWLEDGMENTS

This study was supported by an NSERC grant to M.G.K., and by the Saskatchewan Research Council (D.H.Q.) and the Canadian Light Source (T.G.K., J.N.C.). Research at the PNC-CAT facilities at the APS is supported by the U.S. DOE Office of Science Grant No. DEFG03-97ER45628, the University of Washington, a major facilities access grant from NSERC, Simon Fraser University, and the APS. Use of the APS is also supported by the U.S. Department of Energy, Office of Science, Office of Basic Energy Sciences, under contract no. W-31-109-Eng-38. The authors thank Steve Heald for his help in conducting the experiment at the PNC-CAT facilities. Thanks are also given to Mark Rivers and Steve Sutton (APS GSE-CARS) for their help with XRF quantification software.

REFERENCES CITED

- Bevington, P. (1969) Data reduction and error analysis for the physical sciences. McGraw-Hill, New York.
- Birks, L.S., Gilfrich, J.V., and Criss, J.W. (1977) NRLXRF, A Fortran program for X-ray fluorescence analysis: Users' Guide. Naval Research Laboratory, Washington, D.C., 1977.
- Cabaret, D., Sainctavit, P., Ildefonse, P., and Flank, A.M. (1998) Full multiple scattering calculations of the X-ray absorption near edge structure at the magnesium K-edge in pyroxene. *American Mineralogist*, 83, 300-304.
- Cauzid, J., Philippot, P., Somogyi, A., Simionovici, A., and Bleuett, P. (2004) Quantification of single fluid inclusions by combining synchrotron radiation-induced $\mu\text{-X}$ -ray fluorescence and transmission. *Analytical Chemistry*, 76, 3988-3994.
- Cloutis, E.A. (2002) Pyroxene reflectance spectra: minor absorption bands and effects of chemical substitutions. *Journal of Geophysical Research*, 107, 5039-5049.
- Criss, J.W., Birks, L.S., and Gilfrich, J.V. (1978) Versatile X-ray analysis program combining fundamental parameters and empirical coefficients. *Analytical Chemistry*, 50, 33-37.
- Eng, P.J., Rivers, M.L., Yang, B.X., and Schildkam, W. (1995) Micro-focussing 4 keV to 65 keV X-rays with bent Kirkpatrick-Baez mirrors. *Proceedings of SPIE*, Volume 2516, 41-51.
- Frantz, J.D., Mao, H.K., Zhang, Y.G., Wu, Y., Thompson, A.C., Underwood, J.H., Giauque, R.D., Jones, K.W., and Rivers, M.L. (1988) Analysis of fluid inclu-

- sions by X-ray fluorescence using synchrotron radiation. *Chemical Geology*, 69, 235–245.
- Gunsser, W., Lemke, Th., Rohl, B.R., and Denecke, M.A. (1994) X-ray absorption spectroscopic and magnetic investigations on the garnet $Mn_3Al_{2-x}Cr_xGe_2O_{12}$. *Journal of Solid State Chemistry*, 118, 261–66.
- Gurney, J.J. (1989) Diamonds. In J. Ross, Ed., *Kimberlite and Related Rocks: Their Mantle/Crust Setting, Diamonds, and Diamonds Exploration*. Geological Society of Australia Special Publication, 14, 935–965.
- Gurney, J.J., Harris, J.W. and Rickard, R.S. (1984) Silicate and oxide inclusions in diamonds from the Orapa Mine, Botswana. In J. Kornprobst, Ed., *Kimberlites. The mantle and crust-mantle relationships*, vol. II, p. 3–10. Elsevier, Amsterdam.
- Hansteen, T.H., Sachs, P.M., and Lechtenberg, F. (2000) Synchrotron-XRF microprobe analysis of silicate reference standards using fundamental-parameter quantification. *European Journal of Mineralogy*, 12, 1, 25–31.
- Heald, S., Stern, E., Brewster, D., Gordon, R., Crozier, D., Jiang, D., and Cross, J. (2001) XAFS at the Pacific Northwest Consortium-Collaborative Access Team undulator beamline. *Journal of Synchrotron Radiation*, 8, 342–344.
- Klein, C. and Hurlbut, C. (1993) *Manual of Mineralogy* (after James D. Dana). Wiley, New York.
- Kopylova, M.G., Russell J. K., and Cookenboo H. (1999a) Mapping the Lithosphere Beneath the North Central Slave Craton. *Proceedings of 7th International Kimberlite Conference*, V. 1, Red Roof Design, Cape Town, 468–479.
- — — (1999b) Petrology of peridotite and pyroxenite xenoliths from the Jericho kimberlite: implications for thermal state of the mantle beneath the Slave craton, northern Canada. *Journal of Petrology*, 40, 1, 79–104.
- Levy, D., Artioli, G., Gualtieri, A., Quartieri, S., and Valle, M. (1999) Chromium crystal chemistry mullite-spinel refractory ceramics. *Materials Research Bulletin*, 34, 711–720.
- Mavrogenes, J.A., Bodnar, R.J., Anderson, A.J., Bait, S., Sutton, S.R., and Rivers, M.L. (1995) Assessment of the uncertainties and limitations of quantitative elemental analysis of individual fluid inclusions using synchrotron X-ray fluorescence (SXRF). *Geochimica et Cosmochimica Acta*, 59, 19, 3987–3995.
- McCammon, C. and Kopylova, M.G. (2004) A redox profile of the Slave mantle and oxygen fugacity control in the cratonic mantle. *Contributions to Mineralogy and Petrology*, 148, 55–68.
- Meng, Y., Newville, M., Sutton, S., Rakovan, J., and Mao, H.K. (2003) Fe and Ni impurities in synthetic diamond. *American Mineralogist*, 88, 1555–1559.
- Ohigashi, T., Watanabe, N., Yokosuka, H., Aota, T., Takano, H., Takeuchi, A., and Aoki, S. (2002) Elemental analysis with a full-field X-ray fluorescence microscope and a CCD photon-counting system. *Journal of Synchrotron Radiation*, 9, 128–131.
- Philippot, P., Ménez, B., Chevallier, P., Gibert, F., and Legrand, F., and Populus, P. (1998) Absorption corrections procedures for quantitative analysis of fluid inclusions using synchrotron radiation X-ray fluorescence. *Chemical Geology*, 144, 99–119.
- Quirt, D.H. (2003) *Synchrotron diamond analyses, segment 1: Method testing*. Saskatchewan Research Council, Publication No. 11367-02C03, 31 p plus appendices.
- Rickers, K., Thomas, R., and Heinrich, W. (2004) Trace-element analysis of individual synthetic and natural fluid inclusions with synchrotron radiation XRF using Monte-Carlo simulations for quantification. *European Journal of Mineralogy*, 16, 23–35.
- Seitz, H.M., Brey, G., Stachel, T. and Harris, J., (2003) Li abundances in inclusions in diamonds from the upper and lower mantle. *Chemical Geology*, 201, 307–318.
- Sobolev, N.V., Bartoshinsky, Z.V., Yefimova, E.S., Lavrent'ev, Yu.G., and Pospelova, L.N. (1970) Association of olivine, garnet and chrome-diopside in a Yakutsk diamond. *Doklady. Akademii Nauk SSSR*, 192, 1349–1353 (in Russian).
- Sutton, S.R., Bertsch, P.M., Newville, M., Rivers, M., Lanzirotti, A., and Eng, P. (2002) Microfluorescence and microtomography analyses of heterogeneous earth and environmental materials. In P.A. Fenter, M.L. Rivers, N.C. Sturchio, and S.R. Sutton, Eds., *Applications of synchrotron radiation in low-temperature geochemistry and environmental science*, 49, 429–483. *Reviews in Mineralogy and Geochemistry*, Mineralogical Society of America, Chantilly, Virginia.
- Taura, H., Yurimoto, H., Kurita, K., and Sueno, S. (1998) Pressure dependence on partition coefficients for trace elements between olivine and coexisting melts. *Physics and Chemistry of Minerals*, 25, 469–484.
- Vekemans, B., Vincze, L., Brenker, F.E., and Adams, F. (2004) Processing of three-dimensional microscopic X-ray fluorescence data. *Journal of Analytical and Atomic Spectrometry*, 19, 1302–1308.
- Vincze, L., Vekemans, B., Brenker, F.E., Falkenberg, G., Rickers, K., Somogyi, A., Kersten, M., and Adams, F. (2004). Three-dimensional trace element analysis by confocal X-ray microfluorescence imaging. *Analytical Chemistry*, 76, 6786–6791.

MANUSCRIPT RECEIVED APRIL 7, 2005

MANUSCRIPT ACCEPTED JUNE 20, 2005

MANUSCRIPT HANDLED BY BRYAN C. CHAKOUMAKOS